forests

MDPI

Article

Rapid Operational Mapping of Large Fire Perimeters from Fuel-Specific Aggregation of MODIS and VIIRS Active Fire Detections in Mexico

Carlos Ivan Briones-Herrera [1], Daniel José Vega-Nieva [1*], Jaime Briseño-Reyes [1], Pablito Marcelo López-Serrano [1], José Javier Corral-Rivas [1], Ernesto Alvarado-Celestino [2], Stéfano Arellano-Pérez [3], Enrique J. Jardel Peláez [4], Diego Pérez Salicrup [5], William Matthew Jolly [6]

[1] Facultad de Ciencias Forestales, Universidad Juárez del Estado de Durango, Río Papaloapan y Blvd, Durango S/N Col. Valle del Sur, 34120 Durango, Mexico; carlos.briones.ipi@gmail.com (C.I.B.-H.); normonjaras@gmail.com (N.A.M.-V.); jaime.briseno@gmail.com (J.B.-R.) p_lopez@ujed.mx (P.M.L.-S.); jcorral@ujed.mx (J.J.C.-R.);

[2] School of Environmental and Forest Sciences, University of Washington, Mailbox 352100, University of Washington, Seattle, WA 98195, USA; alvarado@uw.edu

[3] Unidad de Gestión Ambiental y Forestal Sostenible (UXAFORES), Departamento de Ingeniería Agroforestal, Escuela Politécnica Superior de Ingeniería , Universidad de Santiago de Compostela, Campus Universitario s/n, 27002 Lugo, Spain; stefano.arellano@gmail.com (S.A.-P.)

[4] Centro Universitario de la Costa Sur. Universidad de Guadalajara. Av. Independencia Nacional No. 151, Autlán de Navarro, Jalisco, Mexico. enrique.jardel@academicos.udg.mx

[5] Instituto de Investigaciones en Ecosistemas y Sustentabilidad. Universidad Autónoma de México. Antigua Carretera a Pátzcuaro No. 8701 Col. Ex Hacienda de San José de la Huerta C.P. 58190. Morelia, Michoacan, Mexico. diego@cieco.unam.mx

[6] USDA Forest Service, Missoula Fire Sciences Laboratory, Missoula, MT 59808, USA; mjolly@fs.fed.us

* Correspondence: danieljvn@gmail.com (D.J.V.-N.); Tel.: +52-618-183-6804

Received: date; Accepted: date; Published: date

Abstract: Near real time early estimates of burned area are fundamental to forest fire monitoring for improved fire management, including fire emissions quantification. In contrast to available monthly global products of burned area, active fires can allow for early coarse estimates of fire progression in near real time. While some previous studies have suggested potential of active fire aggregation to obtain early estimates of fire progression, there is a need to analyze the effect of fuel types on the active fires aggregated perimeters over long periods of study and large areas of study. In addition, it is necessary to consider the regional variations in the active fires aggregation distance, to implement this technique for an operational monitoring of individual fire and total burned area in near real time. The current study analyzed the effect of contrasted aggregation distances, 750, 1000, 1125 and 1500 m, on the aggregated MODIS and VIIRS active fire perimeters against MODIS MCD64A1 burned area, for a total of 24 fuel types and regions in Mexico, in the period 2012-2018. Optimum aggregation distances varied between fuel types and regions, with the longest aggregation distances of 1500 m observed for the most arid regions and fuel types, dominated by shrubs and grasslands, possibly being associated to a higher fire rate of spread. In contrast, the lowest aggregation distances of 750 and 1,000 m were obtained in the regions and fuel types with the densest forest canopy and wettest climate, possibly dominated by litter fuels and with limitations on fire spread due to fuel moisture. These results demonstrate potential of the active fire detections to characterize fire spread and delineate fire perimeters for a variety of regions and vegetation types. The methodology for the definition of fuel-specific active fire aggregation distance could be replicated for any other region, based on available maps of fuel or vegetation types and ecoregions. This technique could be utilized operationally in early warning and fire danger systems to support fire progression monitoring and fire management decision making in near real time. Future studies might analyze internal variations

within fuel types of fire rates of spread, against medium resolution fire perimeters, for an improved monitoring and prediction of fire progression in near real time.

Keywords: Burned area; forest fuels; MODIS; VIIRS; hotspots; fire monitoring; near-real time.

1. Introduction

An accurate monitoring of burned area dynamics is key to inform fire management planning, including fire prevention, fire suppression decision-making and post-fire impact evaluation, [1-5]. Although the estimation of the area affected by fires is fundamental to carbon cycle and emissions quantification [6-9], large uncertainties still exist in burned area quantification [4,10-16], limiting our ability to quantify fire effects and inform fire management decision making.

Current operational global burned area products [17] are generally available one month after the fire, in contrast with the daily availability of satellite-derived active fire detections data [18-21], limiting their application to support near real time fire monitoring and fire decision making [22-24]. As a consequence, near-real time active fire detection data, are often used as an early estimate of burned area [2,12,14,18,20,25]. For example, global datasets of fire emissions have utilized the relationships between active fire detections and burned area to characterize global dynamics of burned area and fire emissions [18,20,26-28]. These relationships can be particularly useful to account for smaller fires which can be better detected by the thermal anomalies of active fire detections compared to operational coarse burned area products produced using changes in reflectance [2,7].

Consequently, some studies have aimed at developing empirical relationships to predict burned area from the number of active fire detections, at scales ranging from global analysis of coarse resolution (i.e. 0.25 to 0.5°) gridded sum of burned area [2,7,28-30] to regional and local analysis of active fires counts, against coarse to medium resolution satellite burned area or field perimeters, [14,25,31-36]. Such relationships between active fire counts and burned area have been found to vary largely between locations, because of variations between vegetation, topography and weather and associated fire behavior [7,14,18,20,37-39]. For example, Kasischke et al. [38] found that the slope of the relationship of active fire counts with monthly sum of burned area varied between countries (Canada, Alaska and Russia) and within states and provinces; they attributed these variations to regional differences in fire rates of detection, obscuration, and fire rate of spread.

In this sense, some authors have noted that the relationship between active fire counts and burned area is spatially variable and strongly dependent on the vegetation type and function [32,36]. For example, Randerson et al. [7] obtained different coefficients between MODIS sum of burned area and number of MODIS active fires at 0.25° resolution for 5 vegetation types and 14 continental regions analyzed. Furthermore, some authors have been able to utilize satellite estimates of fuel availability, such as cumulative NDVI [29], tree cover [18,20,26], percentage of pasture and shrubland [14] or Leaf Area Index [13] to account for regional variations between active fire counts and sum of burned area, generally at coarse gridded scales of analysis. In addition, some studies have also found the mean size of the monthly active fire clusters to have an effect on the regional relationships between gridded active fire counts and sum of burned area [18,20].

In contrast to these approaches attempting to relate the number of active fires to burned area, other studies have directly tested the potential of various spatial aggregation techniques, to directly map fire perimeters, generally in more local analysis at a fire event scale [40-43]. The techniques tested for directly mapping fire perimeters from aggregated active fires include the direct buffering of active fires [44-46], the use of interpolation techniques such as kriging, inverse distance weighted, or nearest neighbor methods [40,41,43], or the application of convex hull algorithms to active fire clusters [22,24,42,47]. These active fire interpolated perimeters have been validated against coarse [45] and medium scale burned area products produced using changes in reflectance [46], and have even

shown good agreement against daily fire perimeters derived from field data or thermal infrared imagery retrieved from high spatial resolution night-time aerial platforms [40,41,43,44]. Some of these previous analyses have consequently demonstrated the potential of active fire interpolated perimeters for a near real time monitoring of the approximate advance of large fires progression [24,40-43,48]. Furthermore, some studies have utilized interpolated active fire perimeters to initialize, evaluate, and re-calibrate forecasted fire spread from operational fire simulation models [47,49-56] with potential to improve situational awareness and decision making in fire response resources allocation in near real time [23,57]. Most of those previous analyses of active fire aggregated perimeters have focused on the reconstruction of specific fire perimeters, mainly at a local scale of analysis [40-45]. There is, nevertheless, a need for evaluating the technique of active fires aggregation over large periods of study and large areas of study, both for individual fire and total burned area prediction, to quantify its potential for operational use for large scale early mapping of fire activity in near real time [22,24].

In addition, most of the previous literature on fire perimeter delineation from active fires has utilized mainly coarse resolution sensors, generally with 1 km resolution, such as ATSR [38], AVHRR [30-35] or MODIS [36,40-42,44,45,48]. In contrast, the use of the VIIRS active fire product, with an improved spatial resolution (375 m) and higher capacity for small fire detection, still remains relatively unexplored in the literature for direct mapping of fire perimeters [22,43,46].

Moreover, while some global scale studies utilizing active fire counts have shown a role of vegetation types or fuel availability in influencing the relationships between active fires and burned area relationships at coarse scales (0.25-0.5°) [7,14,18,20,26], to our best knowledge, we are not aware of any previous study that has attempted to analyze the role of fuel types on the performance of aggregated active fire clusters to predict burned area, both at individual fire and total monthly burned area levels, over large areas of study. In this sense, the previous study of Briones-Herrera et al. [24] demonstrated the potential of aggregated active fires for mapping monthly burned area at a national level in Mexico, utilizing a single aggregation distance of 1125 m, but it did not analyze potential variations between fuel types or regions. Furthermore, we are not aware of any previous study that has attempted to analyze the potential variations of the optimum aggregation distance of active fires to predict burned area between fuel types and regions with varying conditions of vegetation, climate and anthropogenic characteristics.

The current study aimed to analyze the variations in the best aggregation distance for predicting burned area from MODIS and VIIRS active fires aggregated perimeters, for the main fuel types and regions in Mexico from 2012-2018. Aggregated active fire perimeters at distances of 750, 1000, 1125 and 1500 m, were compared against the current standard MCD64A1 burned area product [17], both at individual fire perimeter level and total sum of burned area, for every fuel type and region of study in the study period. The resulting fuel-specific algorithm for near real time early mapping of large fire perimeters will be integrated in the Forest Fire Forecast Danger System of Mexico [58-60], for supporting the monitoring of large fire progression in near real time to aid in operational fire management decision making.

2. Materials and Methods

2.1. Study Area, fuels and regions data

The area of study was the forest vegetation of the Mexican republic, excluding agricultural lands, water bodies and human settlements, based on the most recent land use map (1: 250,000) INEGI [61] (Figure 1). Fuel types analyzed were based on the fuelbeds map from Jardel-Peláez et al. [62] and on the most recent land use map, series VI (1: 250,000) INEGI [61] (Figure 1).

The term "forest" is used here for natural vegetation areas, with several fuel types dominated by shrubs and/or grassland vegetation, such as desert shrubland, chaparral, natural grasslands, or semi-arid forest (the latter comprised by very open pine and oak forests of low tree cover). Tropical forests

include both seasonally dry and wet forests [62], because of the relatively low number of large fire observations in the latter. Following Briones et al. [24], the regions analyzed were based on the North American level 3 ecoregions map (EPA,), considering the spatial and temporal patterns of fire occurrence observed in previous studies [64-65]. Regions were updated to the most recent land use map (1: 250,000) INEGI [61]. A total of 24 fuel and region types were considered for analysis, as shown in Figure 1.

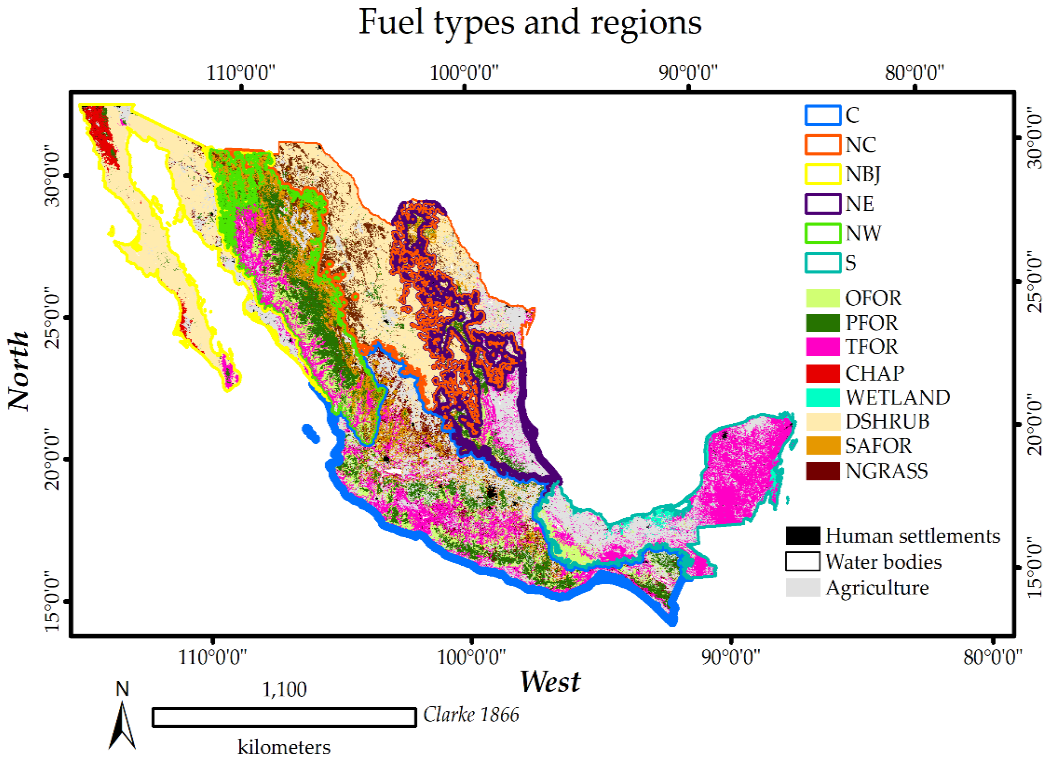


Figure 1. Map of fuelbed types and regions of study. Where: C: Central; NC: North Central; NBJ: North Baja California; NE: Northeast; NW: Northwest; S: South. OFOR: oak forests; PFOR: pine forests; TFOR: tropical forests; CHAP: chaparral forests; WETLAND: wetlands; DSHRUB: desert shrubland forest; SAFOR: semi-arid forests; NGRASS: natural grasslands. Human settlements are shown in black, water bodies, in white and agriculture, in gray, based on the National Institute of Geography and Statistics (INEGI) Land-Use Map Series VI (2014), 1:250,000.

2.2. Burned area and active fires data.

The study period comprised from January 2012 to June 2018. Burned area and active fires data from every month in the period of study were utilized in the analysis. Burned area perimeters from the collection C6 burned area (MCD64A1), with a spatial resolution of 500 m [17], were downloaded from the FTP server of the University of Maryland.

Active fire data from the Moderate Resolution Imaging Radiometer Spectrum (MODIS, C6) [17], and from the Visible Infrared Imaging Radiometer Suite (VIIRS, V1, 375 m) [66] were downloaded from the Fire Information for Resource Management System (FIRMS, https://firms.modaps.eosdis.nasa.gov/download/create.php).

2.2. Predicting Fire Perimeters from the Aggregation of Active Fires by fuels and regions

For the delineation of the active fire perimeters, a convex hull algorithm was applied to monthly MODIS and VIIRS active fires, utilizing the "aggregate points" tool in ArcGIS (ESRI; 2011, Redlands, CA, USA) [67]. Monthly active fire perimeters were calculated at four analyzed aggregation distances: 750, 1000, 1125 and 1500 m. Following Briones-Herrera et al. [24], tested aggregation distances were

based on the spatial resolution of the VIIRS (375 m) and MODIS (1000 m) active fires. The delineation of active fire aggregated perimeters was automated with the arcpy package from the PyCharm 2019.3.1 software (JetBrains, 2017) [68]. The code is available at request to the corresponding author. Aggregated active fire perimeters and burned area MCD64A1 perimeters were combined with the fuel type and region map (Figure 1) and area within each fuel and region was calculated for every active fire and burned area perimeter. Spatially and temporally coinciding MCD64A1 burned area perimeters area were compared with the corresponding interpolated perimeters produced with active fire data in the same location, fuel type and region, utilizing the "spatial join" tool in ArcGIS (ESRI; 2011, Redlands, CA, USA) [67] for every monthly dataset. If several active fire perimeters fell within a MCD64A1 burned area perimeter by fuel type and region, their area was summed for analysis. For each fuel type and region, we used linear regression to compare monthly MCD64A1 burned area with the aggregated active fires perimeter at the four aggregation distances tested, utilizing Equation (1):

$$BA = a * x \quad (1)$$

Where:
BA: MODIS C6 MCD64A1 burned area (ha) by fuel type and region;
a: model parameter; x: aggregated perimeter of active fires (ha) by fuel type and region, respectively.

The models were tested at two levels for each fuel type and region: 1) individual fire perimeter area; 2) total monthly sum of burned area. The best performing models for predicting individual fire area for each fuel type and region, were selected for evaluation at the total monthly sum level. Candidate equations were adjusted utilizing the "lm"package in R (R Core Team, 2017 Vienna, Austria) [69]. The coefficient of determination (R^2), root mean square error (RMSE) and model bias (average of observed minus predicted values) [70] were used to quantify model goodness of fit for every fuel and region dataset, at the two levels of analysis (individual fire and total monthly of burned area). The database for the period of study included a total of 5731 individual monthly fire perimeters. For the monthly sum of burned area evaluation, a total of 79 monthly observations in the study period were utilized.

3. Results

The largest average individual burned area sizes were observed for chaparral and semiarid forest of the NW region, with an average burned area of 1,878 (+/- 3,098) and 1,628 (+/- 3,056) ha, respectively. Lowest individual burned area values were observed for all tropical forests, with individual average fire sizes below 600 ha. Total monthly sum of burned area ranged from 97,6312 (+/- 32,227 ha) for oak forest of the C region to 6,727 (+/- 397) has for tropical forests of the NBJ region. Largest total monthly sum of burned area, of > 400,000 ha, were observed for pine and oak forests of the C and NW regions, semiarid forests of the NW, and tropical forests of the C region, and lowest monthly burned area sums (<20,000 ha) were observed for the more desertic NC and NBJ regions.

Best performing active fire aggregation distances (750, 1000, 1125, 1500 m) varied between the different types of fuel and regions analyzed (Table 1). We also show the slope estimate and confidence interval of the parameters of each model (eq. 1) and the values of the goodness of fit statistics for each fuel type and region (Table 1). Burned area in fuel types dominated by fine fuels, such as chaparral, desert shrubland, natural grasslands, and semi-arid forests, had the best fit with the 1500 m aggregation distance (Table 1). Oak forests burned area had the best fit with 1125 m for C, NE and NW regions, and 1500 for the S region. Best fits for pine forests ranged from 1125 for NW region to 1000 for the NE and 750 m for the C region. For tropical forests, C, S and NBJ regions had the best fit with a 1000 m aggregation distance, while regions of NW and NE, had a best fit at 1500 m (Table 1).

	Individual Fire	**Total Monthly Sum of Burned Area**

Fuel_region	Agg. Dist. (m)	*a*	R^2	RMSE (ha)	bias (ha)	*a*	R^2	RMSE (ha)	bias (ha)
CHAP	1500	1.23(±0.03)	0.94	749	-72	1.14(±0.03)	0.96	971	-53
DSHRUB_NC	1500	0.95(±0.04)	0.69	362	139	0.79(±0.03)	0.89	550	207
DSHRUB_NBJ	1500	2.04(±0.18)	0.70	828	-73	1.67(±0.17)	0.61	969	-59
NGRASS_C	1500	1.28(±0.03)	0.76	382	30	0.74(±0.02)	0.91	1,867	850
NGRASS_NC	1500	1.52(±0.12)	0.77	331	13	1.40(±0.06)	0.95	234	27
NGRASS_NBJ	1500	1.08(±0.16)	0.38	447	189	1.14(±0.14)	0.50	470	58
NGRASS_NW	1500	1.12(±0.09)	0.43	1,781	-79	0.71(±0.08)	0.57	4,552	1,165
OFOR_C	1125	0.81(±0.02)	0.55	689	186	0.57(±0.02)	0.90	10,196	3,377
OFOR_NE	1125	1.13(±0.06)	0.92	304	67	1.11(±0.06)	0.94	442	-11
OFOR_NW	1125	0.91(±0.02)	0.78	517	83	0.75(±0.02)	0.98	3,460	222
OFOR_S	1500	1.17(±0.08)	0.75	368	78	0.86(±0.03)	0.96	344	-22
PFOR_C	750	0.92 (±0.03)	0.46	619	238	0.72(±0.03)	0.92	4,602	1,230
PFOR_NBJ	1500	0.89(±0.08)	0.67	233	-4	0.70(±0.07)	0.63	283	45
PFOR_NE	1000	1.07(±0.10)	0.57	287	107	0.82(±0.07)	0.79	337	123
PFOR_NW	1125	0.85(±0.02)	0.65	678	84	0.59(±0.04)	0.81	10,108	1,528
SAFOR_C	1500	0.46(±0.03)	0.69	729	340	0.45(±0.03)	0.85	2,260	843
SAFOR_NC	1500	0.96(±0.07)	0.78	352	80	0.89(±0.05)	0.90	358	140
SAFOR_NW	1500	0.89(±0.02)	0.88	1,076	69	0.72(±0.03)	0.90	6,952	354
TFOR_C	1000	1.10(±0.03)	0.29	502	208	0.98(±0.02)	0.95	3,431	1,215
TFOR_NBJ	1000	1.00(±0.07)	0.91	156	47	0.78(±0.08)	0.73	205	26
TFOR_NE	1500	0.96(±0.06)	0.74	290	114	0.96(±0.02)	0.98	285	49
TFOR_NW	1500	0.75(±0.04)	0.47	293	74	0.54(±0.03)	0.89	890	201
TFOR_S	1000	0.97(±0.03)	0.46	463	201	0.82(±0.05)	0.85	5,333	639
WET_S	1500	1.30(±0.04)	0.67	788	142	1.07(±0.06)	0.84	3,953	399

Table 1. Coefficients and goodness-of-fit statistics of the best models when comparing burned area with aggregated fire perimeters produced with active fire data for each fuel and region. Where: Fuel_region: fuel type and region (Figure 1); C: Central; NC: North Center; NBJ: North Baja California; NE: Northeast; NW: Northwest; S: South. OFOR: oak forests; PFOR: pine forests; TFOR: tropical forests; CHAP: chaparral forests; WETLAND: wetlands; DSHRUB: desert shrubland forest; SAFOR: semi-arid forests; NGRASS: natural grasslands; Agg. Dist.: best fit aggregation distance (units in meters); Coefficient *a*: is the parameter estimated by the adjusted function (Equation (1)) for the prediction of burned area from the aggregation of active fires by fuel type and region (standard coefficient error shown in parentheses); R^2: coefficient of determination; RMSE: root mean square error (units in ha); bias: model bias (units in ha).

For the individual fire perimeter level, the R^2 was > 0.7 for 11 fuelbeds and > 0.5 for 18 of the 24 fuelbeds analyzed (Table 1). Tropical forests of regions NW, S, and C had some of the lowest goodness of fits, in the range 0.5-0.3. For the total sum of monthly burned area, 11 of the analyzed fuelbeds showed a $R^2 > 0.9$, and 19 of the 24 fuelbeds showed a $R^2 > 0.7$ (Table 1). The fuelbeds with the lowest R^2, in the range 0.6-0.5, for the total sum of monthly burned area were natural grasslands of NW and NBJ regions. (Table 1). Examples of plots of predicted aggregated active fire perimeters, against MODIS MCD64A1 burned area, for individual fire and total monthly sum of burned area are shown in Figure 2.

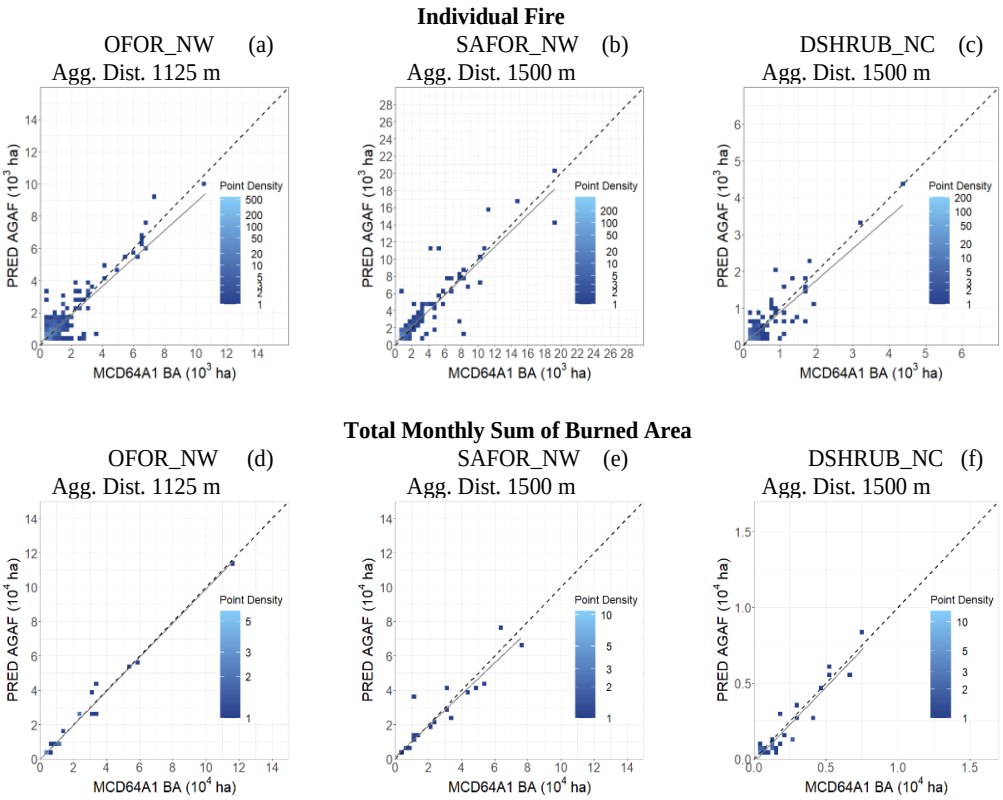


Figure 2. Selected examples of predicted burned area -utilizing eq. 1- from aggregation of active fires against burned area from MCD64A1 for individual perimeters (a,b,c) and for total sum of burned area (d,e,f) at specified aggregation distance. Where: Agg. Dist: Aggregation distance; PRED AGAF: predicted burned area from aggregated active fire perimeter (ha); MCD64A1 BA: MODIS C6 MCD64A1 burned area (ha); OFOR: oak forests; SAFOR: semi-arid forests; DSHRUB: desert shrubland forests; NW: Northwest; NC: North Center; dotted black line represents the 1:1 line and solid gray line represents the observed and predicted correlation regression line. Point density, representing the number of observations by square plot division (in grey) are shown in a blue gradient.

The spatial distribution of the best fit aggregation distances by fuel type and region is mapped in Figure 3. In general, drier areas with higher presence of finer fuels (e.g. chaparral, desert shrubland, natural grasslands, semi-arid forests) showed the highest aggregation distances of 1500 m and intermediate aggregation distances of 1125 m were observed for temperate forests (e.g. pine and oak forests in NW and NE, showed in dark green). The lowest aggregation distances of 750 and 1000 m appear to be mainly in areas dominated by tropical forest, or in temperate forests in the C and S regions, which receive high precipitations.

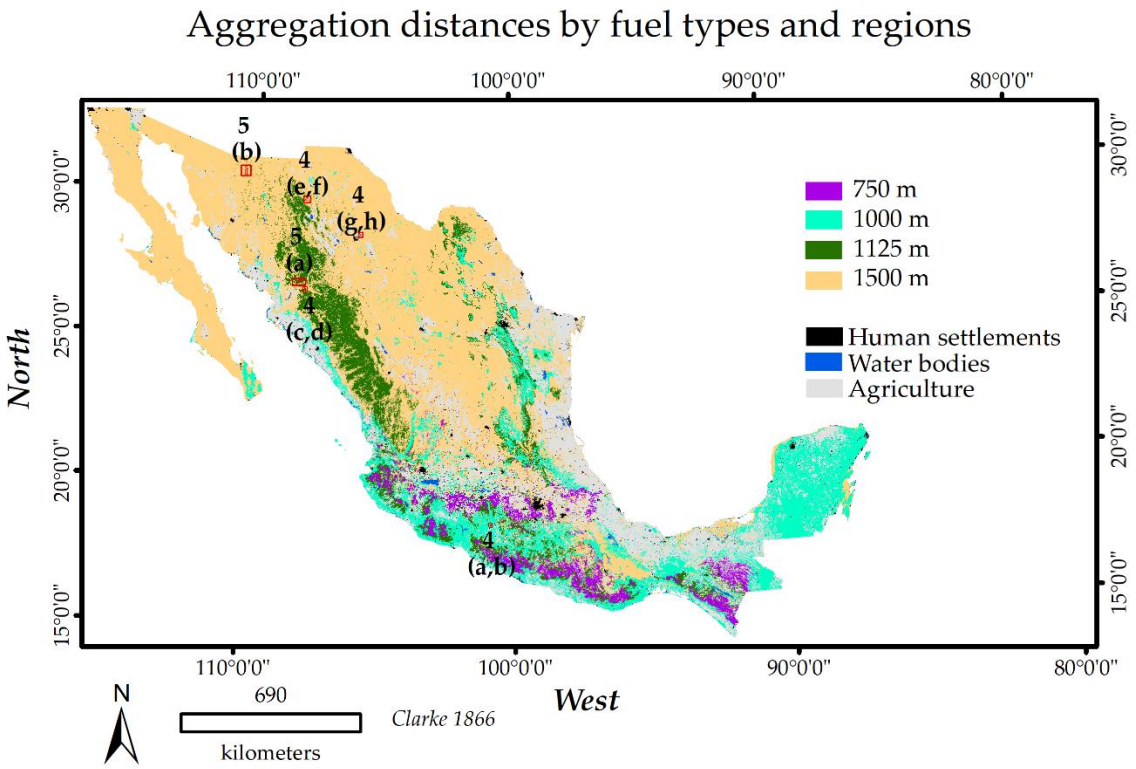


Figure 3. Map of best aggregation distances by fuel types and regions from the best fit models for aggregation of active fires at 750, 1000, 1125 and 1500 m. Human settlements are shown in black, water bodies in navy blue and agriculture in gray, based on the National Institute of Geography and Statistics (INEGI) Land-Use Map Series VI (2014), 1:250,000. The location of detailed windows (Figures 4–5) are shown in red, with the corresponding figure number in black.

Examples comparing aggregated active fires perimeters with MODIS MCD64A1 burned area for selected fuel types and regions with varying aggregation distances are shown in Figure 4. Background colors represent fuel type. The aggregated perimeters could also be mapped on a daily basis or at every satellite acquisition, thereby monitoring large fire progression in near real time [22,24,41,47]. Two selected examples of daily fire progression mapping from aggregated daily active fires are shown for a pine and oak forest fire (Figure 5a) and for a semiarid forest (Figure 5b).

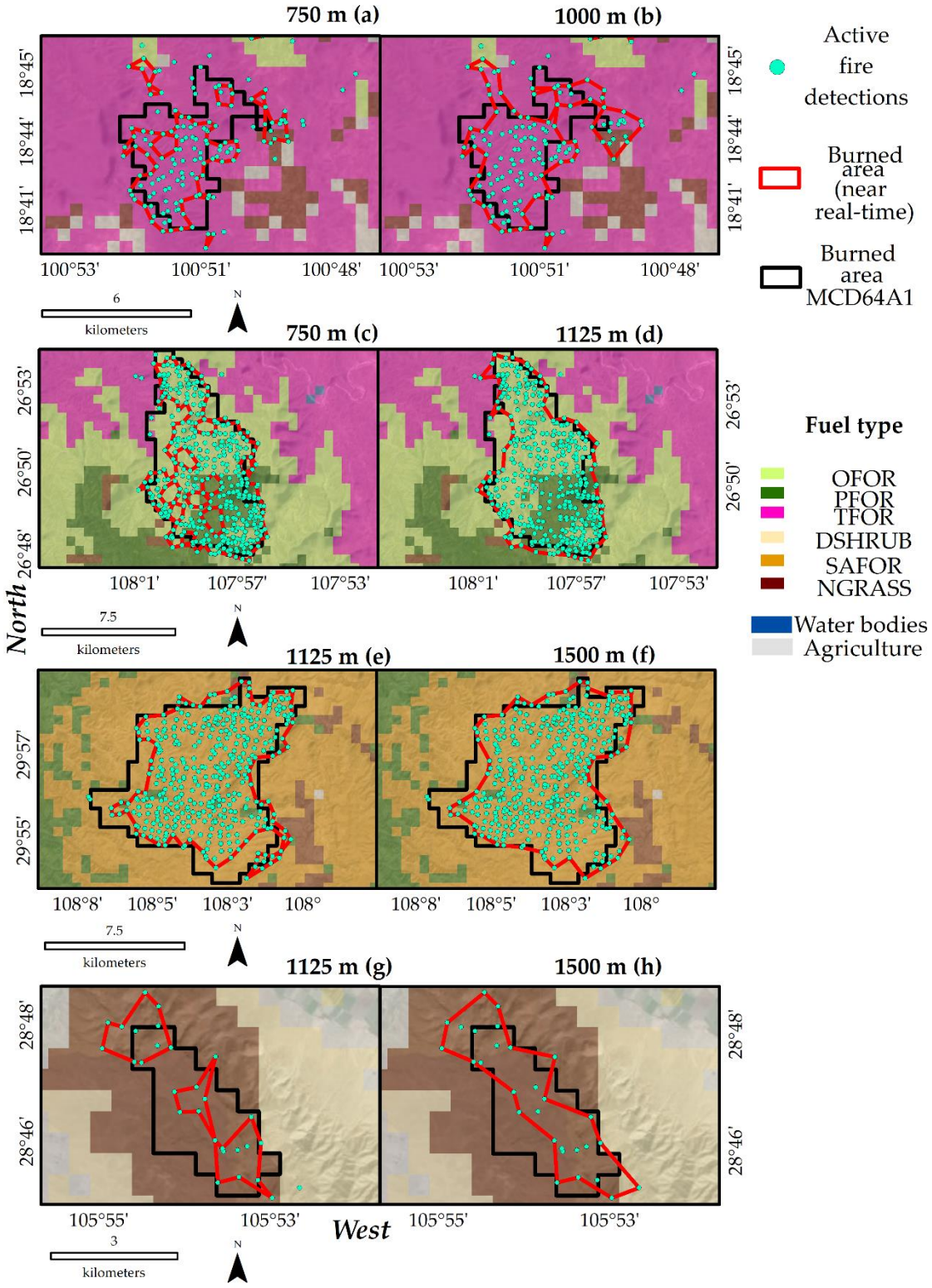


Figure 4. Examples of selected fire perimeters from April 2017 and May 2018 mapped using aggregated MODIS and VIIRS active fire data and MCD64A1 burned area, for tropical forest of the C region (a,b), oak forest of NW region (c,d), semi-arid forest of the NW region (e,f) and grasslands of the NC region (g,h) at different aggregation distances 750 m (a,c); 1000 m (b); 1125 m (d,e) and 1500 m (f,h). MCD64A1 burned areas are shown in black lines, aggregated MODIS and VIIRS active fire perimeters are shown in red. Daily active fire detections are shown in bright blue. Background colors represent fuel types (Figure 1). Water bodies are show in navy blue and agriculture in gray, based on National Institute of Geography and Statistics (INEGI) Land-Use Map Series VI (2014), 1:250,000.

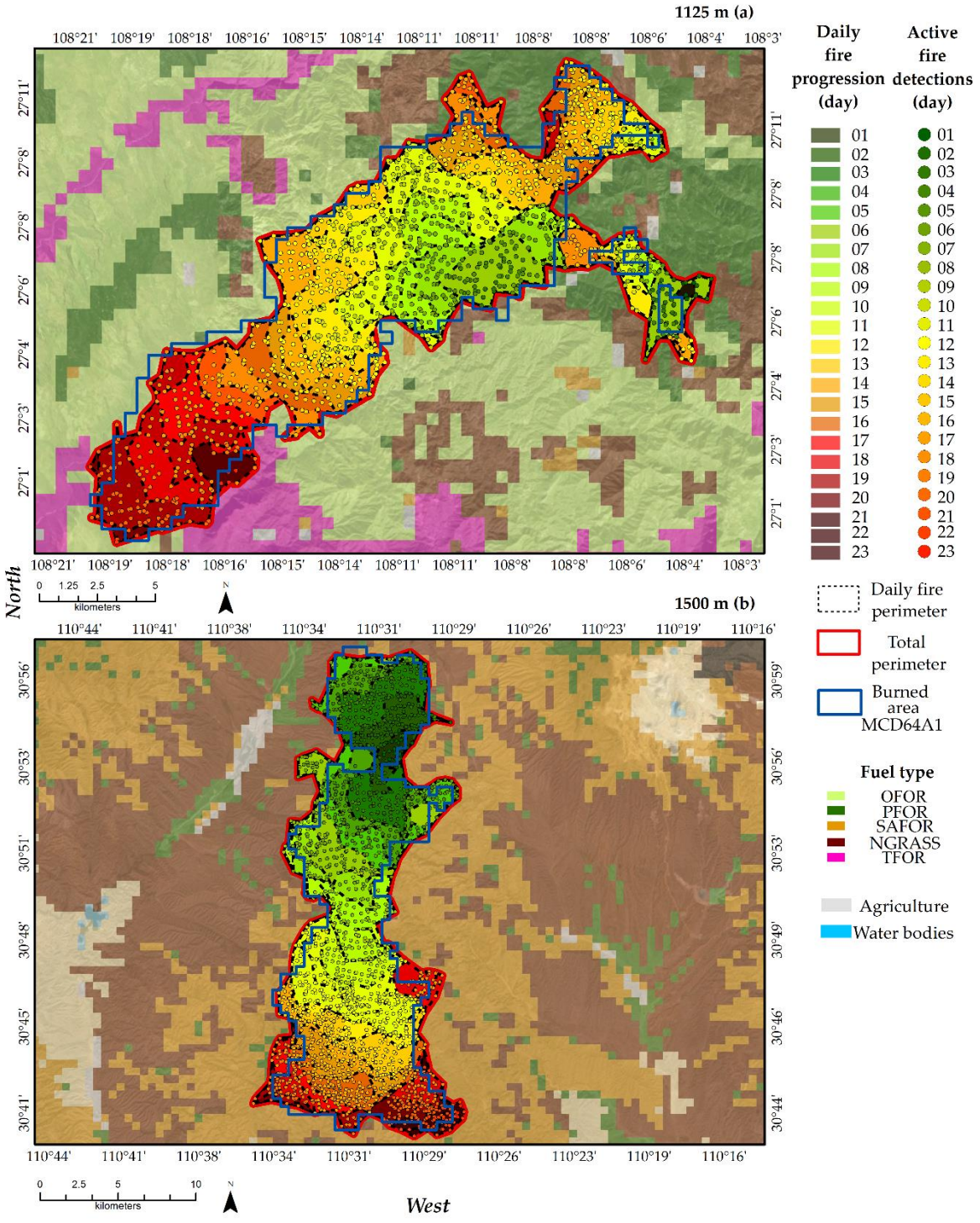


Figure 5. Selected examples of daily fire aggregated perimeters from May 2012 for oak and pine forests of the NW region at 1125 m (a) and from June 2014 for semiarid forests of the NW region at 1500 m (b). Daily fire progression and daily active fire detections are shown in color multiband from green to red, daily fire perimeters are shown in dotted black lines and the total fire perimeter is shown in solid red line. MCD64A1 burned area perimeters are shown in dark blue. Background colors represent fuel types (Figure 1). Water bodies are show in navy blue and agriculture in gray, based on National Institute of Geography and Statistics (INEGI) Land-Use Map Series VI (2014), 1:250,000.

4. Discussion

The results from the current study demonstrated variation between regions of the active fire aggregation distances, agreeing with previous studies that have documented regional variations in the relationships between active fire counts and burned area [7,18,20,37,38,48]. Nevertheless, the approaches utilized, temporal and spatial scale of analysis, and spatial resolution of the satellites utilized here, differed from those previous studies. For example, the global scale analyses of Giglio et al. [18,20] and Randerson et al. [7] developed differentiated models to relate number of active fires to burned area for 14 continental regions at gridded scales of 0.25-0.5°. While this approach is valuable for developing global scale estimates of burned area and emissions [2,28], national level analyses can benefit from finer regionalization and spatial resolutions. In our study at a national scale, the analysis of active fire aggregation between regions suggested a climatic gradient generally corresponds to average fire rate of spread as captured by the active fire aggregation distances (Figure 3). For example, slower spreading fires are more prevalent in areas with higher precipitation such as temperate and tropical forests of the Central and Southern regions (750-1000 m aggregation distance). In contrast, highest rates of active fire spread (1500 m aggregation distance) were found in more arid ecosystems such as the NC, dominated by lower tree canopies and higher shrubs and grass covers. Intermediate average active fire rates of spread (1000-1125 m) were observed for the temperate forests on the NW and NE regions. Interestingly, for some vegetation types such as pine forests, lower rates of average active fire spread were observed for the more humid NE region (1000 m), compared with a relatively higher average rate of spread (1125 m) observed for the pine forests of the NW region, which is characterized by higher fuel dryness conditions [64,65].

In addition to climate, other factors might also be affecting the fire spread potential between regions. For example, the lower fire spread rates found in the C and S regions might be related to limitations in fuel continuity resulting from the high prevalence of agriculture, roads, and human population density [71,72]. This contrasts with a higher spread potential observed in the northern regions that is potentially related to less human infrastructure and higher fuel connectivity [72]. The results from the current study seem to confirm the potential of active fires to characterize fire rate of spread between regions (e.g. [48]) and could provide valuable inputs for further analysis of fire regimes, including size, and rate of spread, between ecoregions of contrasting human and climatic characteristics [3,73-76]. Such a future analysis of fire size and spread potential against human, climatic and vegetation factors, including a formal evaluation of the role of fuel connectivity [77,78], might help further clarify the driving factors of fire propagation between regions.

A strong effect of fuel type was observed in our study, thereby corroborating previously reported observations at coarse scales that fuel availability influenced differences in the relationships between active fires and burned area [14,18,20,26,29]. For all of the regions analyzed, vegetation characterized by a higher fine fuel availability, such as chaparral, desert shrubland, natural grassland and semiarid forests, consistently showed the highest active fire aggregation distances, very possibly caused by the well-documented effect of fine fuels on increasing rate of fire spread, compared to lower rate of spread fuel types in more dense tree cover forests [62,79-83]. To our best knowledge, this is the first study to quantify such fuel-specific variations utilizing MODIS and VIIRS aggregated active fire perimeters. This said, our results agree with the general patterns of fuel availability-related effects of tree cover or percentage of grass and shrubs [14,18,20,26] observed in previous coarse scale analysis. For example, at a 0.5° resolution analysis, previous studies found that elevated NDVI [29] or tree cover [26] corresponded to a reduced number of active fire detections per effective burned area. Similarly, our results also agree with the finding of Hanstson et al. [14] who found that increasing percentage of shrubs and grassland or decreasing percentage of forest cover increased the slope of the relationship between the total sum of burned area and the number of active fires in 10 Landsat scenes. While our results agree with those previous analyses in also suggesting a positive effect of fine fuel on active fire spread, in this case it was quantified for both total burned area sum and individual fire perimeter levels, utilizing finer resolution active fires and scales of analysis.

The results from the current study confirm the potential of active fire aggregation techniques to develop early estimates of fire perimeters [22,40-43], thereby supporting fire management decision making in near real time (e.g. [23,57]). Previous studies utilizing convex hull aggregation of fire perimeters [22,24,42] did not aim at analyzing the effect of aggregation distance on the capacity of burned area perimeter delineation between fuels. In contrast, this study, as far as we know, is the first to quantify the effect of fuel types and regions on the fire aggregation distance for fire perimeter delineation and does so over a large spatial and temporal domain. The technique shows potential for operational application for near real time early mapping of approximate fire progression [22,24] and future work will test its operational GIS integration in the Forest Fire Forecast Danger System of Mexico [58-60] for supporting near real time fire monitoring and fire management operational decision support making. The methodology presented in this study could be replicated elsewhere, based on near real time available active fire data, combined with available maps of types of vegetation [84,85] or fuel types [86].

Ongoing research for calibrating Sentinel images (resolution=10-20m) to map fire perimeters and severity over a variety of fuel types and regions in Mexico [60,87] will likely allow comparisons of the procedure described in this paper to finer resolution perimeters [24,46,88]. Fire perimeters produced using active fire detections might improve to some extent the evaluation of small fire burned area compared to the coarse resolution burned area products [7,24]. Meanwhile, a regression against medium resolution perimeters for the smallest burns, characterized by 1 or 2 active fire detections, which do not result in an interpolated coarse scale perimeter utilizing aggregation algorithms [24], might be required for a detailed evaluation of the contribution of smallest burns in total burned area [15].

Future studies might also analyze further variability in fire rates of spread by additionally considering variations of tree cover [89], aboveground biomass [90-92] or tree height [93]. This analysis, together with a characterization of fire radiative power (FRP) [94-97] across fuel types and tree cover levels could potentially be useful for refining fuel mapping and improving fire behavior predictions [59,60]. In this sense, the effects of seasonal or daily weather variations [7,48,95,97-99], including effects of wind on fire rate of spread (e.g.[100]), might be considered in future analysis. In addition, daily variations in fire rate of spread as quantified with aggregated perimeters could be used to initialize and re-calibrate fire spread models (e.g.[47,50-53,55,101]). Lastly, such data-driven tools that are initialized and calibrated with active fire data could potentially support near real time forecasting of fire progression and behavior to orient operational fire management decision making (e.g.[23,47,57]).

5. Conclusions

This study demonstrated the potential of accounting for the role of fuel type for defining the best aggregation distances when delineating near real time large fire perimeters from aggregated active fires, thereby supporting operational forest fire monitoring and fire management decision making. The highest active fire aggregation distances were necessary for fuel types dominated by shrubs or grasslands, such as chaparral, desert shrubland, or semiarid forests. In contrast, the lowest distances were used for denser canopy temperate and tropical forests where fire spread is expected to be limited by a lower fine fuel availability. Our results support the general trend of increasing burned area per active fire with increasing fine fuel presence that has been observed in previous coarse scale studies with gridded active fire counts. Our approach therefore quantified the relationship between area burned and active fire detections at a fairly fine spatial scale and did so by using point aggregation techniques at an individual fire perimeter and total sum of burned levels. In addition to fuel types, the distance of aggregation varied between regions of contrasting climatic and human presence conditions, a topic that deserves further research to quantify the human and climatic drivers of fire spread, including fuel connectivity limitations imposed by human activity. The analysis

presented here could be replicated for any other region to derive fuel and region specific near real time estimates of fire extent based on active fires and available vegetation or fuel type maps.

Future studies could focus on analyzing aggregated active fire perimeters against medium resolution perimeters, taking into account potential variations of fire rate of spread caused by internal variability in tree cover, height or aboveground biomass within fuel types, potentially improving both fuel classification and associated fire spatial hazard characterization and mapping. The role of weather, including topographically corrected wind, on explaining variations in fire spread, could be further quantified in future studies. Those future studies could aim both at improving fire perimeter monitoring, possibly at daily time scales, and also at initializing, calibrating and improving fire spread forecast models, with the potential to support fire management decision making in near real time.

Author Contributions: Conceptualization, Carlos Ivan Briones-Herrera and Daniel José Vega-Nieva; Formal analysis, Carlos Ivan Briones-Herrera, Norma Angélica Monjarás-Vega , Jaime Briseño-Reyes; Methodology, Daniel José Vega-Nieva, Pablito Marcelo López-Serrano and José Javier Corral-Rivas; Software, Jaime Briseño-Reyes ; Writing – original draft, Daniel José Vega-Nieva and Carlos Ivan Briones-Herrera; Writing – review & editing, Ernesto Alvarado-Celestino, Stéfano Arellano-Pérez, Enrique J. Jardel Peláez, Diego Pérez Salicrup, William Mathew Jolly and Sean A. Parks.

Funding: Funding for this study was provided by CONAFOR/CONACYT Projects "CO2-2014-3-252620" and "CO-2018-2-A3-S-131553" for the development and enhancement of a Forest Fire Danger Prediction System for Mexico, funded by the Sectorial Fund for forest research, development and technological innovation "Fondo Sectorial para la investigación, el desarrollo y la innovación tecnológica forestal".

Acknowledgments: We would like to thank CONAFOR's personnel for their support to the current study and their continuous feedback for the development of the Forest Fire Forecast Danger System of Mexico (CONAFOR, 2020). The scholarship from CONACYT for Carlos Briones to study a doctoral program in Forest Sciences at the Universidad Juarez del Estado de Durango, is also acknowledged.

Conflicts of Interest: The authors declare no conflict of interest. The founding sponsors had no role in the design of the study; in the collection, analyses, or interpretation of data; in the writing of the manuscript, and in the decision to publish the results.

References

1. Eidenshink, J.; Schwind, B.; Brewer, K.; Zhu, Z.L.; Quayle, B.; Howard, S. A project for monitoring trends in burn severity. *Fire Ecol*. **2007**, *3*, 3–21
2. Van der Werf, G.R.; Randerson, J.T.; Giglio, L.; van Leeuwen, T.T.; Chen, Y.; Rogers, B.M.; Mu, M.; van Marle, M.J.E.; Morton, D.C.; Collatz, G.J.; e al. Global fire emissions estimates during 1997–2016. *Earth Syst. Sci. Data.* **2017**, *9*, 697–720, doi:10.5194/essd-9-697-2017.
3. Andela, N.; Morton, D.C.; Giglio, L.; Paugam, R.; Chen, Y.; Hantson, S.; van der Werf, G.R.; Randerson, J.T. The Global Fire Atlas of individual fire size, duration, speed and direction. *Earth. Syst. Sci. Data*. **2019**, *11*, 529–552, doi:10.5194/essd-11-529-2019, 2019.
4. Chuvieco, E.; Mouillot, F.; Guido, R.; van der Werf.; San-Miguel-Ayanz, J.; Tanase, M.; Koutsias, N.; García, M.; Yebra, M.; Padilla, M.; Gitas, I.; et al. Historical background and current developments for mapping burned area from satellite Earth observation. *Remote Sens. Environ*. **2019**, *225*, 45–64, ISSN 0034-4257, doi:10.1016/j.rse.2019.02.013.
5. Hawbaker, T.J.; Vanderhoof, M.K.; Schmidt, G.L.; Beal, Y.; Picotte, J.J.; Takacs, J.D.; Falgout, J.T.; Dwyer, J.L. The Landsat Burned Area algorithm and products for the conterminous United States, *Remote Sens. Environ.* **2020**, *244*, 2020, 111801, ISSN 0034-4257, https://doi.org/10.1016/j.rse.2020.111801.
6. Giglio, L.; Randerson, J.T.; van der Werf, G.R., Kasibhatla, P.S., Collatz, G.J., Morton, D.C., DeFries, R.S. Assessing variability and long-term trends in burned area by merging multiple satellite fire products. *Biogeosciences*. **2010**, *7*, 1171–1186.
7. Randerson, J.T.; Chen, Y.; van der Werf, G.R.; Rogers, B.M.; Morton, D.C. Global burned area and biomass burning emissions from small fires. *J. Geophys. Res*. **2012**, *117*, G04012, doi:10.1029/2012JG002128.

8. Yue, C.; Ciais, P.; Cadule, P.; Thonicke, K.; Archibald, S.; Poulter, B.; Hao, W.; Hantson, S.; Mouillot, F.; Friedlingstein, P. Modelling the role of fires in the terrestrial carbon balance by incorporating SPITFIRE into the global vegetation model ORCHIDEE–part 1: simulating historical global burned area and fire regimes. *Geosci. Model Dev.* **2014**, *7*, 2747–2767
9. Knorr, W.; Jiang, L.; Arneth, A. Climate, CO2 and human population impacts on global wildfire emissions. *Biogeosciences*. **2016**, *13*, 267.
10. Boschetti, L.; Eva, H.; Brivio, P. A.; Grégoire, J.M.. Lessons to be learned form the intercomparison of three satellite-derived biomass burning datasets. *Geophys. Res. Lett.* **2004**, *31*, (21), L21501. doi:10.1029/2004GL021229
11. Silva, J.M.N.; Sá, A.C.L.; Pereira, J.M.C. Comparison of burned area estimates derived from SPOTVEGETATION and Landsat ETM+ data in Africa: Influence of spatial pattern and vegetation type, *Rem. Sens. Environm.* **2005**, 96, 188–201, ISSN 0034-4257, doi:10.1016/j.rse.2005.02.004.
12. Smith, R.; Adams, M.; Maier, S.; Craig, R.; Kristina, A.; Maling, I. Estimating the area of stubble burning from the number of active fires detected by satellite. *Rem. Sens. Environm.* **2007**, *109*, 95–106.
13. Roy, D.; Boschetti, L.; Justice, C.O.; Ju, J. The Collection 5 MODIS Burned Area Product–Global evaluation by comparison with the MODIS active fire product. *Rem. Sens. Environm*. **2008**, *112*, 3690–3707. 10.1016/j.rse.2008.05.013.
14. Hantson, S.; Padilla, m.; Corti, D.; Chuvieco, E. Strengths and weaknesses of MODIS hotspots to characterize global fire occurrence. *Remote Sens. Environ.* **2013**, *131*, 152–159, ISSN 0034-4257.
15. Roteta, E.; Bastarrika, A.; Padilla, M.; Storm, T.; Chuvieco, E. Development of a Sentinel-2 burned area algorithm: Generation of a small fire database for sub-Saharan Africa. *Remote Sens. Environ.* **2019**, 222, 1–17, ISSN 0034-4257, doi:10.1016/j.rse.2018.12.011.
16. Scholtz, R.; Prentice, J.; Tang, Y.; Twidwell, D. Improving on MODIS MCD64A1 Burned Area Estimates in Grassland Systems: A Case Study in Kansas Flint Hills Tall Grass Prairie. *Remote Sens.* **2020**, *12*, 2168.
17. Giglio, L.; Boschetti, L.; Roy, D.P.; Humber, M.L.; Justice, C.O. The Collection 6 MODIS burned area mapping algorithm and product. *Remote Sens. Environ.* **2018**, *217*, 72–85, ISSN 0034-4257.
18. Giglio, L.; van der Werf, G.R.; Randerson, J.T.; Collatz, G.J.; Kasibhatla, P. Global estimation of burned area using MODIS active fire observations. *Atmos. Chem. Phys.* **2006a**, *6*, 957–974, doi:10.5194/acp-6-957-2006.
19. Giglio, L.; Csiszar, I.; Justice, C.O. Global distribution and seasonality of active fires as observed with the Terra and Aqua Moderate Resolution Imaging Spectroradiometer (MODIS) sensors. *J. Geophys. Res.* **2006b**, *111*, G02016, doi:10.1029/2005JG000142.
20. Giglio, L.; Randerson, J.T.; van der Werf, G.R., Kasibhatla, P.S., Collatz, G.J., Morton, D.C., DeFries, R.S. Assessing variability and long-term trends in burned area by merging multiple satellite fire products. *Biogeosciences* **2010**, *7*, 1171–1186.
21. Giglio, L.; Schroeder, W.; Justice, C.O. The collection 6 MODIS active fire detection algorithm and fire products. *Remote Sens. Environ.* **2016**, 178, 31–41, ISSN 0034-4257, doi:10.1016/j.rse.2016.02.054.
22. Artés, T.; Boca, R.; Liberta, G.; San-Miguel-Ayanz, J. Non-supervised method for early forest fire detection and rapid mapping, Proc. SPIE 10444. In Proceedings of the Fifth International Conference on Remote Sensing and Geoinformation of the Environment (RSCy2017), 104440R, 20–23 March **2017**, Paphos, Cyprus, doi:10.1117/12.2280714.
23. Ramirez, J.; Monedero, S.; Silva, C.A.; Cardil, A. Stochastic decision trigger modelling to assess the probability of wildland fire impact, *Sci. Total Environ.* **2019**, *694*, 133505, ISSN 0048-9697, doi:10.1016/j.scitotenv.2019.07.311.
24. Briones-Herrera, C.I.; Vega-Nieva, D.J.; Monjarás-Vega, N.A.; Briseño-Reyes, J.; López-Serrano, P.M.; Corral-Rivas, J.J.; Alvarado-Celestino, E.; Arellano-Pérez, S.; Álvarez-González, J.G.; Ruiz-González, A.D.; Jolly, W.M.; Parks, S.A. Near Real-Time Automated Early Mapping of the Perimeter of Large Forest Fires from the Aggregation of VIIRS and MODIS Active Fires in Mexico. *Remote Sens*. **2020**, *12*, 2061.
25. Loboda, T. and Csiszar, I. Estimating burned area from AVHRR and MODIS: Validation results and sources of errors. Proceeding of the 2nd Open All-Russia Conference: Current aspects of remote sensing of earth from space. **2005**, (pp. 415–421). Moscow, Russia: Space Research Institute of the Russian Academy of Sciences, Publishing house GRANP.
26. Van der Werf, G.R.; Randerson, J.T.; Collatz, G.J.; Giglio, L. Carbon emissions from fires in tropical and subtropical ecosystems. *Glob. Change Biol.* **2003**, *9*, 547-562, doi:10.1046/j.1365-2486.2003.00604. x.

27. Van der Werf, G. R., J. T. Randerson, L. Giglio, G. J. Collatz, M. Mu, P. S. Kasibhatla, D. C. Morton, R. S. DeFries, Y. Jin, and T. T. van Leeuwen. Global fire emissions and the contribution of deforestation, savanna, forest, agricultural, and peat fires (1997–2009), *Atmos. Chem. Phys*. **2010,** *11*, 707-735, doi:10.5194/acp-10-11707-2010.
28. Giglio, L.; Randerson, J.T.; van der Werf, G.R. Analysis of daily, monthly, and annual burned area using the fourth generation global fire emissions database (GFED4). *J. Geophys. Res. Biogeosci*. **2013**, *118*, 317–328.
29. Scholes, R. J., Kendall, J. D., and Justice, C. O. The quantity of biomass burned in southern Africa, *J. Geophys. Res. Atmos.* **1996**, *101*, *23* 667–23 676.
30. Pereira, J.M.; Pereira, B.S.; Barbosa, P.; Stroppiana, D.; Vasconcelos, M.J.P.; Gregoire, J.M. Satellite monitoring of fire in the EXPRESSO study area during the 1996 dry season experiment: Active fires, burnt area, and atmospheric emissions. *J. Geophys. Res.-Atmos*. **1999**, *104*(D23), 30 701–30 712, 1999.
31. Randriambelo, T.; Baldy, S.; Bessafi, M.; Petit, M.; Despinoy, M. An improved detection and characterization of active fires and smoke plumes in south-eastern Africa and Madagascar, *Int. J. Rem. Sens*. **1998**, *19*(14), 2623–2638, 1998.
32. Nielsen, T.T.; Mbow, C.; Kane, R. A statistical methodology for burned area estimation using multitemporal AVHRR data. *Int. J. Remote Sens.* **2002**, *23*, 1181–1196.
33. Li, Z.; Nadon, S.; Cihlar, J. Satellite-based detection of Canadian boreal forest fires: Development and application of the algorithm. *Int. J. Remote Sens.* **2000a**, *21*, 3057-3069.
34. Li, Z., S.; Nadon, J. Chilar, and B. Stocks**.** Satellite-based mapping of Canadian boreal forest fires: Evaluation and comparison of algorithms. *Int. J. Remote Sens.* **2000b**, *21*, 3071–3082.
35. Sukhinin, A.I.; French, N.H.F.; Kasischke, E.S.; Hewson, J.H.; Soja, A.J.; Csiszar, I.A.; Hyer, E.J.; Loboda, T.; Conrad, S.G.; Romasko, V.I.; et al. AVHRR-based mapping of fires in Russia: New products for fire management and carbon cycle studies. *Rem. Sens. Environm.* **2004**, *93*, 546–564.
36. Tansey, K.; Beston, J.; Hoscilo, A.; Page, S.E.; Paredes-Hernández, C.U. Relationship between MODIS fire hot spot count and burned area in a degraded tropical peat swamp forest in Central Kalimantan, Indonesia. *J. Geophys. Res.* **2008**, *113*, D23112.
37. Eva, H. and Lambin, E.F. Remote sensing of biomass burning in tropical regions: Sampling issues and multisensor approach. *Remote Sens. Environ.* **1998**, *64*, 292–315.
38. Kasischke, E.S.; Hewson, J.H.; Stocks, B.; van der Werf, G.; Randerson, J. The use of ATSR active fire counts for estimating relative patterns of biomass burning a study from the boreal forest region. *Geophys. Res. Lett*. **2003**, 30, 1969, doi:10.1029/2003GL017859, 18.
39. van der Werf, G.R.; Randerson, J.T.; Giglio, L.; Collatz, G.J.; Kasibhatla, P.S.; Arellano, A.F., Jr. Interannual variability of global biomass burning emissions from 1997 to 2004. *Atmos. Chem. Phys. Discuss. Eur. Geosci. Union* **2006**, *6*, 3175–3226.
40. Veraverbeke, S.; Sedano, F.; Hook, S.J.; Randerson, J.T.; Jin Yufang, J.; Brendan, R.M. Mapping the daily progression of large wildland fires using MODIS active fire data. *Int. J. Wildland Fire*. **2014**, 23, 655–667.
41. Parks, S.A. Mapping day-of-burning with coarse resolution satellite fire-detection data. *Int. J. of Wildland Fire.* **2014a,** *23*:215–223
42. Chiaraviglio, N.; Artés, T.; Bocca, R.; Lopez-Pérez, J.; Gentile, A.; San-Miguel-Ayanz, J.; Cortés, A.; Margalef, T. Automatic fire perimeter determination using MODIS hotspots information. 12th Int. Conf. e-Sci. (e-Science) **2016**, 414–423. IEEE.
43. Scaduto, E.; Chen, B.; Jin, Y. Satellite-Based Fire Progression Mapping: A Comprehensive Assessment for Large Fires in Northern California. *IEEE J. Selected Topics in Applied Earth Obs. Remote Sens.* **2020**, *13*, 5102-5114, doi: 10.1109/JSTARS.2020.3019261.
44. Salmon, J.M.; Hao, W.M.; Miller, M.E.; Nordgren, B.; Kaufman, Y. Li, R. Validation of two MODIS single-scene fire products for mapping burned area: hot spots and NIR spectral test burn scars. 4th International Workshop on Remote Sensing and GIS Applications to Forest Fire Management: Innovative Concepts and Methods in Fire Danger Estimation. Emilio Chuvieco, Pilar Martín and Chris Justice (Editors). Ghent – Belgium, 5-7 June **2003**
45. Henderson, S.B.; Ichoku, C.; Burkholder, B.J.; Brauer, M.; Jackson, P.L. The validity and utility of MODIS data for simple estimation of area burned and aerosols emitted by wildfire events. *Int. J. Wildland Fire.* **2010**, *19*, 844–852.
46. Oliva, P. and Schroeder, W. Assessment of VIIRS 375m active fire detection product for direct burned area mapping. *Rem. Sens. Environm.* **2015**, *160*, 144–155.

47. Cardil, A.; Monedero, S.; Ramírez, J.; Silva, C.A. Assessing and reinitializing wildland fire simulations through satellite active fire data. *J. Environ. Manag.* **2019a**, *231*, 996–1003, doi:10.1016/j.jenvman.2018.10.115.
48. Loboda, T.V. and Csiszar, I.A. Reconstruction of fire spread within wildland fire events in Northern Eurasia from the MODIS active fire product. *Glob. Planet. Change*. **2007**, *56*, 258–273, ISSN 0921-8181, doi:10.1016/j.gloplacha.2006.07.015.
49. Anderson, K.R.; Englefield, P.; Little, J.M.; Reuter, G. An approach to operational forest fire growth predictions for Canada. *Int. J. Wildland. Fire*. **2009**, *18*, 893–905.
50. Coen, J.L. and Schroeder, W. Use of spatially refined satellite remote sensing fire detection data to initialize and evaluate coupled weather-wildfire growth model simulations. *Geophys. Res. Lett*. **2013**, *40*, 5536–5541
51. Mandel, J.; Beezley, J.D.; Kochanski, A.K.; Kondratenko, V.Y.; Kim, M. Assimilation of perimeter data and coupling with fuel moisture in a wildland fire – Atmosphere DDDAS. *Procedia Comput. Sci.* **2012**, *9*, 1100-1109
52. Mandel, J.; Kochanski, A.K.; Vejmelka, M.; Beezley, J. D. Data assimilation of satellite fire detection in coupled atmosphere-fire simulations by WRF-SFIRE. In; Advances in Forest Fire Research, D.X. Viegas, Ed., *Coimbra University Press*, **2014**, 716-724
53. Sá, A.C.L.; Benali, A.; Fernandes, P.M.; Pinto, R.M.S.; Trigo, R.M.; Salis, M.; Russo, A.; Jerez, S.; Soares, P.M.; Schroeder, W.; et al. Evaluating fire growth simulations using satellite active fire data. *Rem. Sens. Environm.* **2017**, *190*, 302–317.
54. Benali, A.; Sa, A.C.L.; Ervilha, A.R.; Trigo, R.M., Fernandes, P.M.; Pereira, J.M.C. Fire spread predictions: Sweeping uncertainty under the rug. *Sci. Total Environ.* **2017**, *592*, 187–196, doi:10.1016/j.scitotenv.2017.03.106.
55. Farguell Caus, A.; Haley, J.; Kochanski, A.K.; Cortés Fité, A.; Mandel, J. Assimilation of fire perimeters and satellite detections by minimization of the residual in a fire spread model. *Lecture Notes in Comput. Sci*. **2018**, *10861*, 711–723. doi: 10.1007/978-3-319-93701-4_56
56. Monedero, S.; Ramirez, J.; Cardil, A. Predicting fire spread and behaviour on the fireline. Wildfire analyst pocket: A mobile app for wildland fire prediction. *Ecol. Model*. **2019**, *392*, 103-107.
57. Pinto, M.M.; Renata, M.S.; Benali, A.; Sá, A.C.L.; Fernandes, P.M.; Soares, P.M.M.; Cardoso, R.M.; Trigo, R.M.; Pereira, J.M.C. Probabilistic fire spread forecast as a management tool in an operational setting. *Springerplus* **2016**, *5*, 1205, doi:10.1186/s40064-016-2842-9.
58. CONAFOR, 2020. Sistema de Predicción de Peligro de Incendios Forestales de México. **2020**, Available online at: http://forestales.ujed.mx/incendios2/ (Last accessed November 17th 2020)
59. Vega-Nieva, D.J.; Nava-Miranda, M.G.; Calleros-Flores, E.; López-Serrano, P.M.; Briseño-Reyes, J.; Corral-Rivas, J.J.; Cruz-López, M.I.; Cuahutle, M.; Ressl, R.; Alvarado-Celestino, E. et al., The Forest Fire Danger Prediction System of Mexico. **2019a.** Proceedings for the 6th International Fire Behavior and Fuels Conference April 29 – May 3, 2019, Albuquerque, New Mexico USA. Ed. International Association of Wildland Fire, Missoula, Montana, USA. Available online at: http://albuquerque.firebehaviorandfuelsconference.com/wp-content/uploads/sites/13/2019/04/DANIEL-JOSE-VEGA-NIEVA-Albuquerque.pdf
60. Vega-Nieva, D.J.; Nava-Miranda, M.G.; Calleros-Flores, E.; López-Serrano, P.M.; Briseño-Reyes, J.; Corral-Rivas, J.J.; Cruz-López, M.I.; Cuahutle, M.; Ressl, R.; Alvarado-Celestino, E. et al., The Forest Fire Danger Prediction System of Mexico. The Forest Fire Danger Prediction System of Mexico. Remote Sensing Early Warning Systems: Virtual Wildfire Workshop. **2020**. 6-8 October 2020. Ed. Commission for Environmental Cooperation (CEC). http://forestales.ujed.mx/incendios2/php/publicaciones_documentos/Vega20_v2_The_Forest_Fire_Danger_Prediction_System_of_Mexico.pdf (Last accessed November 17th 2020)
61. INEGI (Instituto Nacional de Estadística y Geografía-México). Guía Para la Interpretación de Cartografía: Uso del suelo y Vegetación. escala 1, 250, 000: Serie VI; Instituto Nacional de Estadística y Geografía: Ciudad de México, México, **2014**.
62. Jardel-Peláez, E.J.; Alvarado, E.; Quintero-Gradilla, S.D.; Rodríguez-Gómez, J.M.; Pérez-Salicrup, D.; Michel-Fuentes, J.M.; Castillo-Navarro, M.F. Fuel beds and fire potential in Mexican terrestrial ecosystems. *Fire Ecol.* **2020**. under review.

63. United States Environmental Protection Agency. Ecoregions of North America. https://www.epa.gov/eco-research/ecoregions-north-america (Last accessed November 17th 2020)
64. Vega-Nieva, D.J.; Nava-Miranda, M.G.; Calleros-Flores, E.; López-Serrano, P.M.; Briseño-Reyes, J.; Corral-Rivas, J.J.; Cruz-López, M.I.; Cuahutle, M.; Ressl, R.; Alvarado-Celestino, E. et al., Developing Models to Predict the Number of Fire Hotspots from an Accumulated Fuel Dryness Index by Vegetation Type and Region in Mexico. *Forests*, **2018**, *9*, 190. DOI: 10.3390/f9040190
65. Vega-Nieva, D.J.; Nava-Miranda, M.G.; Calleros-Flores, E.; López-Serrano, P.M.; Briseño-Reyes, J.; Corral-Rivas, J.J.; Cruz-López, M.I.; Cuahutle, M.; Ressl, R.; Alvarado-Celestino, E. et al., Temporal patterns of fire density by vegetation type and region in Mexico and its temporal relationships with a monthly satellite fuel greenness index. *Fire Ecol.* **2019b**, *15*, 28. DOI: 10.1186/s42408-019-0042-z
66. Schroeder, W.; Oliva, P.; Giglio, L.; Csiszar, I. The New VIIRS 375 m active fire detection data product: Algorithm description and initial assessment. *Rem. Sens. Environm.* **2014**, *143*, 85–96. 10.1016/j.rse.2013.12.008.
67. ESRI. ArcGIS Desktop 10.1; Environmental Systems Research Institute: Redlands, CA, USA, **2011**.
68. JetBrains. Pycharm. **2017**, [online] JetBrains. Available online: https://www.jetbrains.com/pycharm/ (accessed on 16 October 2020).
69. R Core Team. R: A Language and Environment for Statistical Computing; R Foundation for Statistical Computing: Vienna, Austria. Available online: https://www.R-project.org/ (accessed on 20 March 2017).
70. Ryan, T.P. Modern Regression Methods. In Wiley Series in Probability and Statistics; John Wile and Sons: New York, NY, USA, **1997**; 515p.
71. Pompa-García, M.; Camarero, J.J.; Rodríguez-Trejo, D.A.; Vega-Nieva, D.J. Drought and spatiotemporal variability of forest fire across Mexico. *Chinese Geographical Science*, **2018**, *28*, 25-37 DOI: 10.1007/s11769-017-0928-0
72. Monjarás-Vega, N.A.; Briones-Herrera, C.I.; Vega-Nieva, D.J.; Calleros-Flores, E.; Corral-Rivas, J.J.; López- Serrano, P.M.; Pompa-García, M.; Rodríguez-Trejo, D.A.; Carrillo-Parra, A.; González-Cabán, A.; et al. Predicting forest fire kernel density at multiple scales with geographically weighted regression in Mexico. *Sci. Total. Environ*. **2020**, *718*, 137313, doi:10.1016/j.scitotenv. 2020.137313
73. Chuvieco, E., Giglio, L., & Justice, C.O.: Global characterization of fire activity: toward defining fire regimes from Earth observation data. *Global Change Biol*., **2008**, *14*, 1488–1502, doi:10.1111/j.1365-2486.2008.01585.x, 2008.
74. Archibald, S.; Roy, D.P.; van Wilgen, B.W.; Scholes, R.J. What limits fire? An examination of drivers of burnt area in Southern Africa. Glob. Chang. Biol. **2009**, 15, 613–630.
75. Parks, S.A.; Parisien, M.A.; Miller, C.; Dobrowski, S.Z. Fire activity and severity in the western US vary along proxy gradients representing fuel amount and fuel moisture. *Plos One*. **2014b**, 9:e99699.
76. Parisien, M.A.; Miller, C.; Parks, S.A.; DeLancey, E.R. The spatially varying influence of human on fire probability in North America. *Environ. Res. Lett.* **2016**, *11*,7, 075005.
77. Fernandes, P.M.; Monteiro-Henriques, T.; Guiomar, N.; Loureiro, C.; Barros, A.M. Bottom-up variables govern large-fire size in Portugal. *Ecosystems*. **2016**, *19*(8), 1362-1375.
78. Kahiu, M.N. and Hanan, N.P. Fire in subSaharan Africa: The fuel, cure and connectivity hypothesis. *Glob. Ecol. Biogeogr*. **2018**, *27*, 8, 946-957.
79. Scott, J.H. and Burgan, R.E. Standard fire behavior fuel models: a comprehensive set for use with Rothermel's surface fire spread model. Gen. Tech. Rep. RMRS-GTR-153. Fort Collins, CO: U.S. Department of Agriculture, Forest Service, Rocky Mountain Research Station. **2005**, 72 p.
80. Anderson, W.R.; Cruz, M.G.; Fernandes, P.M.; McCaw, W.L.; Vega, J.A.; Bradstock, R.A.; Fogarty, L.; Gould, J.; McCarthy, G.; Marsden-Smedley, J.B.; et al. A generic, empirical-based model for predicting rate of fire spread in shrublands. *Int. J. Wildl. Fire.* **2015**, *24*, 443-460
81. Rodríguez-Trejo, D.A. Incendios de Vegetación su Ecología e Historia. Vol 2. Biblioteca Básica de Agricultura. Guadalajara, Jalisco, Mexico. Printings Arts. **2015**, *2*, ISBN: 9-786077-152378
82. Rodríguez-Trejo, D. A.; Pulido-Luna, J. A.; Martínez-Muñoz, P.; Martínez-Lara, P. J.; Monjarás-Vega, N. A. Comparative analysis of prescribed burns applied to tropical oak woodlands. *Agrociencia.* **2018,** *52*(6), 783-801
83. Rodríguez-Trejo, D.A., Martínez Muñoz, P., Pulido Luna, J.A., Martínez Lara, P.J., & Cruz López, J.D. Combustibles, comportamiento del fuego y emisiones en un pastizal y una sabana artificiales en Chiapas. *Rev. Biol. Trop*. **2020,** *68*(2), 641-654.

84. Friedl, M.A.; Sulla-Menashe, D.; Tan, B.; Schneider, A.; Ramankutty, N.; Sibley, A.; Huang, X. MODIS Collection 5 global land cover: Algorithm refinements 460 and characterization of new datasets. *Remote Sens. Environ*. **2010**, *114*, 168–182. 461 doi:10.1016/j.rse.2009.08.016
85. ESA, European Space Agency. CCI Land Cover Product User Guide version 2.4. **2014**, 449 ESA CCI LC project.
86. Pettinari, M.L. and Chuvieco, E. Generation of a global fuel data set using the Fuel Characteristic Classification System, *Biogeosciences*. **2016**, *13*, 2061–2076, https://doi.org/10.5194/bg-13-2061-2016, 2016.
87. Silva Cardoza, A.I. Evaluation and mapping of forest fires severity in the Western Sierra Madre, Mexico. In: Proceedings of the XIV Congreso Mexicano de Recursos Forestales, Durango, Mexico, 6– November **2019**.
88. Llorens, R., Sobrino, J. A., Fernández, C., Fernández-Alonso, J. M., & Vega, J. A. A methodology to estimate forest fires burned areas and burn severity degrees using Sentinel-2 data. Application to the October 2017 fires in the Iberian Peninsula. *Int. J. Appl. Earth Obs. Geoinf.* **2020**, *95*, 9. https://doi.org/10.1016/j.jag.2020.102243
89. Sexton, J.O.; Song, X.-P.; Feng, M.; Noojipady, P.; Anand, A.; Huang, C.; Kim, D.-H.; Collins, K.M.;Channan, S.; DiMiceli, C.; et al. Global, 30-m resolution continuous fields of tree cover: Landsat-based rescaling of MODIS vegetation continuous fields with lidar-based estimates of error. *Int. J. Digit. Earth*. **2013**, *6*, 427–448.
90. Cartus, O.; Kellndorfer, J.; Walker, W.; Franco, C.; Bishop, J.; Santos, L.; Fuentes, J.M.F. A national, detailed map of forest aboveground carbon stocks in Mexico. *Remote Sens*. **2014**, *6*, 5559-5588. DOI: 10.3390/rs6065559
91. Rodriguez-Veiga, P., Saatchi, S., Tansey, K., Balzter, H., Magnitude, spatial distribution and uncertainty of forest biomass stocks in Mexico. *Remote Sens. Environ.* **2016,** *183,* 265–281.
92. Briones-Herrera, C.I.; Vega-Nieva, D.J.; Monjarás-Vega, N.A.; Flores-Medina, F.; Lopez-Serrano, P.M.; Corral-Rivas, J.J.; Carrillo-Parra, A.; Pulgarin-Gámiz, M.A.; Alvarado-Celestino, E.; González-Cabán, A.; Arellano-Pérez, S.; Álvarez-González, J.G.; Ruiz-González, A.D.; Jolly, W.M. Modeling and mapping forest fire occurrence from aboveground carbon density in Mexico. *Forests*. **2019**, *10*, 402. DOI: doi.org10.3390/f10050402
93. Potapov, P.; Li, X.; Hernandez-Serna, A.; Tyukavina, A.; Hansen, C.M.; Kommareddy, A.; Pickens, A.; Turubanova, S.;Tang, H.; Silva, C.E.; Armston, J.; Dubayah, R.; Blair, J.B.; Hofton, M. Mapping global forest canopy height through integration of GEDI and Landsat data, *Remote Sens. Environ.* **2020**, 112165, ISSN 0034-4257, https://doi.org/10.1016/j.rse.2020.112165.
94. Ichoku, C.; Giglio, L.; Wooster, M. J.; Remer, L.A. Global characterization of biomass-burning patterns using satellite measurements of fire radiative energy. *Remote Sens. Environ.* **2008**, 112(6), 2950−2962.
95. Jolly, W.M. and Freeborn, P.H. Towards Improving Wildland Firefighter Situational Awareness Through Daily Fire Behaviour Risk Assessments In The US Northern Rockies And Northern Great Basin. *Int. J. Wildl. Fire*. **2017**, *26*, 574–586. DOI: 10.1071/WF16153
96. Johnston, J.M.; Wooster, M.J.; Paugam, R.; Wang, X.; Lynham, T.J.; Johnston, L.M. Direct estimation of byram's fire intensity from infrared remote sensing imagery. *Int. J. Wildland Fire*, **2017**, *26*, 668–684.
97. Jolly, W.M.; Freeborn, P.H.; Page, W.G.; Butler, B.W. Severe Fire Danger Index: A Forecastable Metric to Inform Firefighter and Community Wildfire Risk Management. *Fire*. **2019**, *2*, 47.
98. Freeborn, Patrick H.; Cochrane, Mark A.; Jolly, W. Matt. Relationships Between Fire Danger And The Daily Number And Daily Growth Of Active Incidents Burning In The Northern Rocky Mountains, USA. . *International Journal of Wildland Fire* **2015,** *24*, 900–910. doi:10.1071/WF14152
99. Giuseppe, D.F.; Rémy, S., Pappenberger, F., and Wetterhall, F.: Using the Fire Weather Index (FWI) to improve the estimation of fire emissions from fire radiative power (FRP) observations, *Atmos. Chem. Phys.* **2018**, *18*, 5359–5370, https://doi.org/10.5194/acp-18-5359-2018, 2018.
100. Billmire, M.; French, N.H.F.; Loboda, T.; Owen, R.C.; Tyner, M. Santa Ana winds and predictors of wildfire progression in southern California. *Int. J. Wildland Fire.* **2014**, *23*, 1119-1129.
101. Cardil, A.; Monedero, S.; Silva, C.A.; J. Ramirez. Adjusting the rate of spread of fire simulations in realtime. *Ecol. Model.* **2019b**, *395*, 39–44.



© 2020 by the authors. Submitted for possible open access publication under the terms and conditions of the Creative Commons Attribution (CC BY) license (http://creativecommons.org/licenses/by/4.0/).